Computational Mechanics 32 (2003) 40–51 © Springer-Verlag 2003
DOI 10.1007/s00466-003-0460-1

An interaction integral method for analysis of cracks in orthotropic functionally graded materials

B. N. Rao, S. Rahman

Abstract This paper presents two new interaction integrals for calculating stress-intensity factors (SIFs) for a stationary crack in two-dimensional orthotropic functionally graded materials of arbitrary geometry. The method involves the finite element discretization, where the material properties are smooth functions of spatial co-ordinates and two newly developed interaction integrals for mixed-mode fracture analysis. These integrals can also be implemented in conjunction with other numerical methods, such as meshless method, boundary element method, and others. Three numerical examples including both mode-I and mixed-mode problems are presented to evaluate the accuracy of SIFs calculated by the proposed interaction integrals. Comparisons have been made between the SIFs predicted by the proposed interaction integrals and available reference solutions in the literature, generated either analytically or by finite element method using various other fracture integrals or analyses. An excellent agreement is obtained between the results of the proposed interaction integrals and the reference solutions.

Keywords Crack, Orthotropic functionally Graded materials, Finite element method, Stress-intensity factor, *J*-integral, Interaction integral

1 Introduction

In recent years, functionally graded materials (FGMs) have been introduced and applied in the development of structural components subject to non-uniform service requirements. FGMs, which possess continuously varying microstructure and mechanical and/or thermal properties, are essentially two-phase particulate composites, such as ceramic and metal alloy phases, synthesized such that the composition of each constituent changes continuously in one direction, to yield a predetermined composition profile [1]. Even though the initial developmental emphasis of FGMs was to synthesize thermal barrier coating for space applications [2], later investigations uncovered a wide variety of potential applications, including nuclear fast breeder reactors [3], piezoelectric and thermoelectric devices [4–6], graded refractive index materials in audio-video disks [7], thermionic converters [8], dental and medical implants [9], and others [10]. The absence of sharp interfaces in FGM largely reduces material property mismatch, which has been found to improve resistance to interfacial delamination and fatigue crack propagation [11]. However, the microstructure of FGM is generally heterogeneous, and the dominant type of failure in FGM is crack initiation and growth from inclusions. The extent to which constituent material properties and microstructure can be tailored to guard against potential fracture and failure patterns is relatively unknown. Such issues have motivated much of the current research into the numerical computation of crack-driving forces and the simulation of crack growth in FGMs.

Analytical work on functionally graded materials begins as early as 1960 when soil was modeled as a non-homogeneous material by Gibson [12]. Thereafter, extensive research on various aspects of isotropic FGMs fracture under mechanical [13–15] or thermal [16–22] loads has been carried out by various investigators. Crack problems under both mode-I [23, 24] and mixed mode [25, 26] loading conditions were studied using finite element method (FEM) and J_k^*-integral method. Gu et al. [27] presented a simplified method for calculating the crack-tip field of FGMs using the equivalent domain integral technique. Bao and Wang [28] studied multi-cracking in an FGM coating. Bao and Cai [29] studied delamination cracking in a functionally graded ceramic/metal substrate. Kim and Paulino [26] evaluated the mixed-mode fracture parameters in FGMs using FEM analysis with three different approaches: the path-independent J_k^*-integral method, the modified crack-closure integral method, and the displacement correlation technique. In the J_k^*-integral method [16, 26], there is need to perform integration along the crack face of the discontinuity (e.g., in calculating J_2^*). Recently, Rao and Rahman [30] developed two new interaction integrals in conjunction with the element-free Galerkin method for mixed-mode fracture analysis in isotropic FGM. Dolbow and Gosz [31] have also derived a similar path independent interaction integral method. However, most analytical methods reviewed above are developed to quantify crack-driving force in isotropic FGMs.

Given the nature of processing techniques, graded materials can become anisotropic. For example, graded materials processed by a plasma spray technique generally

Received: 28 February 2002 / Accepted: 23 May 2003

B. N. Rao (✉), S. Rahman
Center for Computer-Aided Design,
The University of Iowa, Iowa City,
IA 52242–1000, USA
E-mail: bnrao@ccad.uiowa.edu

The authors would like to acknowledge the financial support of the U.S. National Science Foundation (NSF) under Award No. CMS-9900196. The NSF program director was Dr. Ken Chong.

have a lamellar structure [32], whereas processing by electron beam physical vapor deposition would lead to a highly columnar structure [33]. Such materials would not be isotropic, but orthotropic with material directions that can be considered perpendicular to one other as an initial approximation. Gu and Asaro [34] performed theoretical studies on a four-point bend specimen consisting of orthotropic FGMs with a fluctuating Poisson's ratio. Ozturk and Erdogan [35, 36] used integral equations to investigate mode-I and mixed-mode crack problems in an infinite nonhomogeneous orthotropic medium with the crack aligned with one of the material directions, and a constant Poisson's ratio. Recently, Kim and Paulino [37] employed the FEM for fracture analysis of orthotropic FGMs involving the modified crack-closure (MCC) and the displacement correlation technique (DCT). Hence, there is considerable interest in developing efficient method for extracting appropriate crack-driving force in orthotropic FGMs.

This paper presents two new interaction integrals for calculating the fracture parameters of a stationary crack in orthotropic FGM of arbitrary geometry. This method involves FEM, where the material properties are smooth functions of spatial co-ordinates and two newly developed interaction integrals for mixed-mode fracture analysis. In conjunction with the proposed method, both mode-I and mixed-mode two-dimensional problems have been solved. Three numerical examples are presented to evaluate the accuracy of SIFs calculated by the proposed method. Comparisons have been made between the SIFs predicted by the proposed method and the existing results available in the current literature.

2
Crack tip fields in orthotropic FGM

Consider a plane problem in rectilinear anisotropic elasticity. The basic equations that describe the deformation of anisotropic materials are the same as those for isotropic materials except for the adoption of a generalized Hooke's law. The most general anisotropic form of linear elastic stress-strain relation is given by

$$\varepsilon_{ij} = S_{ijkl}\sigma_{kl} \quad (i,j,k,l = 1,2,3) \tag{1}$$

where σ_{kl} is the stress tensor, ε_{ij} is the strain tensor, and S_{ijkl} is the fourth-order compliance tensor. Due to the symmetry of σ_{kl} and ε_{ij}, 81 independent components of the compliance tensor reduces to 36 independent components. The existence of a strain energy function provides a further reduction in the number of independent components to 21 ($S_{ijkl} = S_{klij}$). In order to represent S_{ijkl} in compact form, a contracted notation a_{ij} is introduced as follows:

$$\varepsilon_i = \sum_{j=1}^{6} a_{ij}\sigma_j \quad i,j = 1,2,\ldots,6 \tag{2}$$

where a_{ij} are compliance coefficients with $a_{ij} = a_{ji}$ and

$$\begin{aligned} &\varepsilon_1 = \varepsilon_{11},\ \ \varepsilon_2 = \varepsilon_{22},\ \ \varepsilon_3 = \varepsilon_{33},\\ &\varepsilon_4 = 2\varepsilon_{23},\ \ \varepsilon_5 = 2\varepsilon_{13},\ \ \varepsilon_6 = 2\varepsilon_{12}\\ &\sigma_1 = \sigma_{11},\ \ \sigma_2 = \sigma_{22},\ \ \sigma_3 = \sigma_{33},\\ &\sigma_4 = \sigma_{23},\ \ \sigma_5 = \sigma_{13},\ \ \sigma_6 = \sigma_{12}\ . \end{aligned} \tag{3}$$

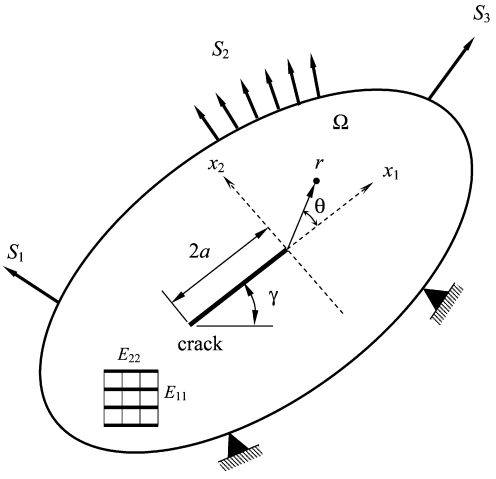

Fig. 1. A crack in an orthotropic functionally graded material

At each point through the thickness of transversely isotropic materials there is a plane of material symmetry that runs parallel to the plane of the problem. For this special case, the compliance coefficients in Eq. (2) can be reduced to depend upon six independent elastic constants, $a_{ij}\ i,\ j = 1,2,6$ for plane stress conditions and $b_{ij} = a_{ij} - \frac{a_{i2}a_{j3}}{a_{33}}\ i,\ j = 1,2,6$ for plane strain conditions.

Figure 1 shows a crack tip that is referred to the Cartesian coordinate system in orthotropic FGMs. Two dimensional anisotropic elasticity problems can be formulated in terms of the analytic functions $\phi_j(z_j)$ of the complex variable $z_j = x_j + iy_j (j = 1,2)$, where

$$x_j = x + \alpha_j y, \quad y_j = \beta_j y \qquad (j = 1,2) \tag{4}$$

The parameters α_j and β_j are the real and imaginary parts of $\mu_j = \alpha_j + i\beta_j$, which can be determined from [38]

$$a_{11}\mu^4 - 2a_{16}\mu^3 + (2a_{12} + a_{66})\mu^2 - 2a_{26}\mu + a_{22} = 0 \tag{5}$$

The roots μ_j are always either complex or purely imaginary in conjugate pairs as $\mu_1, \bar{\mu}_1, \mu_2$, and $\bar{\mu}_2$. Hence, the linear-elastic singular stress field near the crack tip can be obtained as [39]

$$\sigma_{11} = \frac{1}{\sqrt{2\pi r}}\left[K_I f_{11}^I(\mu_1,\mu_2,\theta) + K_{II} f_{11}^{II}(\mu_1,\mu_2,\theta)\right]\ , \tag{6}$$

$$\sigma_{22} = \frac{1}{\sqrt{2\pi r}}\left[K_I f_{22}^I(\mu_1,\mu_2,\theta) + K_{II} f_{22}^{II}(\mu_1,\mu_2,\theta)\right]\ , \tag{7}$$

$$\sigma_{12} = \frac{1}{\sqrt{2\pi r}}\left[K_I f_{12}^I(\mu_1,\mu_2,\theta) + K_{II} f_{12}^{II}(\mu_1,\mu_2,\theta)\right]\ , \tag{8}$$

where $f_{ij}^I(\mu_1,\mu_2,\theta)$ and $f_{ij}^{II}(\mu_1,\mu_2,\theta)$ (i, j = 1, 2) are the standard angular functions for a crack in an orthotropic elastic medium, given by

$$f_{11}^I(\mu_1,\mu_2,\theta) = \mathrm{Re}\left[\frac{\mu_1\mu_2}{\mu_1-\mu_2}\left(\frac{\mu_2}{\sqrt{\cos\theta + \mu_2\sin\theta}} - \frac{\mu_1}{\sqrt{\cos\theta + \mu_1\sin\theta}}\right)\right]\ , \tag{9}$$

$$f_{11}^{II}(\mu_1,\mu_2,\theta)=\mathrm{Re}\left[\frac{1}{\mu_1-\mu_2}\left(\frac{\mu_2^2}{\sqrt{\cos\theta+\mu_2\sin\theta}}-\frac{\mu_1^2}{\sqrt{\cos\theta+\mu_1\sin\theta}}\right)\right]\ , \tag{10}$$

$$f_{22}^{I}(\mu_1,\mu_2,\theta)=\mathrm{Re}\left[\frac{1}{\mu_1-\mu_2}\left(\frac{\mu_1}{\sqrt{\cos\theta+\mu_2\sin\theta}}-\frac{\mu_2}{\sqrt{\cos\theta+\mu_1\sin\theta}}\right)\right]\ , \tag{11}$$

$$f_{22}^{II}(\mu_1,\mu_2,\theta)=\mathrm{Re}\left[\frac{1}{\mu_1-\mu_2}\left(\frac{1}{\sqrt{\cos\theta+\mu_2\sin\theta}}-\frac{1}{\sqrt{\cos\theta+\mu_1\sin\theta}}\right)\right]\ , \tag{12}$$

$$f_{12}^{I}(\mu_1,\mu_2,\theta)=\mathrm{Re}\left[\frac{\mu_1\mu_2}{\mu_1-\mu_2}\left(\frac{1}{\sqrt{\cos\theta+\mu_1\sin\theta}}-\frac{1}{\sqrt{\cos\theta+\mu_2\sin\theta}}\right)\right]\ , \tag{13}$$

$$f_{12}^{II}(\mu_1,\mu_2,\theta)=\ \mathrm{Re}\left[\frac{1}{\mu_1-\mu_2}\left(\frac{\mu_1}{\sqrt{\cos\theta+\mu_1\sin\theta}}-\frac{\mu_2}{\sqrt{\cos\theta+\mu_2\sin\theta}}\right)\right]\ . \tag{14}$$

The near tip displacement field $\mathbf{u}=\{u_1,u_2\}^{\mathrm{T}}$ can be obtained as [39]

$$u_1=\sqrt{\frac{2r}{\pi}}\left[K_I g_1^I(\mu_1,\mu_2,\theta)+K_{II}g_1^{II}(\mu_1,\mu_2,\theta)\right]\ , \tag{15}$$

and

$$u_2=\sqrt{\frac{2r}{\pi}}\left[K_I g_2^I(\mu_1,\mu_2,\theta)+K_{II}g_2^{II}(\mu_1,\mu_2,\theta)\right]\ , \tag{16}$$

where $g_i^I(\mu_1,\mu_2,\theta)$ and $g_i^{II}(\mu_1,\mu_2,\theta)$, i = 1, 2 are the standard angular functions for a crack in an orthotropic elastic medium, given by

$$g_1^I(\mu_1,\mu_2,\theta)=\mathrm{Re}\left[\frac{1}{\mu_1-\mu_2}\left(\mu_1 p_2\sqrt{\cos\theta+\mu_2\sin\theta}-\mu_2 p_1\sqrt{\cos\theta+\mu_1\sin\theta}\right)\right]\ , \tag{17}$$

$$g_1^{II}(\mu_1,\mu_2,\theta)=\mathrm{Re}\left[\frac{1}{\mu_1-\mu_2}\left(p_2\sqrt{\cos\theta+\mu_2\sin\theta}-p_1\sqrt{\cos\theta+\mu_1\sin\theta}\right)\right]\ , \tag{18}$$

$$g_2^I(\mu_1,\mu_2,\theta)=\mathrm{Re}\left[\frac{1}{\mu_1-\mu_2}\left(\mu_1 q_2\sqrt{\cos\theta+\mu_2\sin\theta}-\mu_2 q_1\sqrt{\cos\theta+\mu_1\sin\theta}\right)\right]\ , \tag{19}$$

$$g_2^{II}(\mu_1,\mu_2,\theta)=\mathrm{Re}\left[\frac{1}{\mu_1-\mu_2}\left(q_2\sqrt{\cos\theta+\mu_2\sin\theta}-q_1\sqrt{\cos\theta+\mu_2\sin\theta}\right)\right]\ . \tag{20}$$

In Eqs. (6–20), μ_1 and μ_2 denote the crack-tip parameters calculated as the roots of Eq. (5), which are taken such that $\beta_j>0$ $(j=1,2)$, and p_j and q_j are given by

$$p_j=a_{11}\mu_j^2+a_{12}-a_{16}\mu_j\ , \tag{21}$$

$$q_j=a_{12}\mu_j+\frac{a_{22}}{\mu_j}-a_{26}\ . \tag{22}$$

Even though the material gradient does not influence the square-root singularity or the singular stress distribution, the material gradient does affect the SIFs. Hence, the fracture parameters are functions of the material gradients, external loading, and geometry.

3 The interaction integral method

The interaction integral method is an effective tool for calculating mixed-mode fracture parameters in homogeneous orthotropic materials [40, 41]. In this section the interaction integral method for homogeneous orthotropic materials is first briefly summarized, then extended for cracks in orthotropic FGM. In fact, the study of orthotropic FGM would enhance the understanding of a fracture in a generic material, since upon shrinking the gradient layer in FGM is expected to behave like a sharp interface, and upon expansion, the fracture behavior would be analogous to that of an orthotropic homogeneous material.

3.1 Homogeneous materials

The path independent J-integral for a cracked body is given by [42]

$$J=\int_\Gamma\left(W\delta_{1j}-\sigma_{ij}\frac{\partial u_i}{\partial x_1}\right)n_j\partial\Gamma\ , \tag{23}$$

where $W=\int\sigma_{ij}\,\mathrm{d}\varepsilon_{ij}$ is the strain energy density and n_j is the jth component of the outward unit vector normal to an arbitrary contour Γ enclosing the crack tip. For linear-elastic material models it can shown that $W=\sigma_{ij}\varepsilon_{ij}/2=\varepsilon_{ij}D_{ijkl}\varepsilon_{kl}/2$, where D_{ijkl} are the components of the constitutive tensor. Applying the divergence theorem, the contour integral in Eq. (23) can be converted into an equivalent domain form, given by [43]

$$J=\int_A\left(\sigma_{ij}\frac{\partial u_i}{\partial x_1}-W\delta_{1j}\right)\frac{\partial q}{\partial x_j}\mathrm{d}A+\int_A\frac{\partial}{\partial x_j}\left(\sigma_{ij}\frac{\partial u_i}{\partial x_1}-W\delta_{1j}\right)q\,\mathrm{d}A\ , \tag{24}$$

where A is the area inside the contour and q is a weight function chosen such that it has a value of *unity* at the crack tip, *zero* along the boundary of the domain, and arbitrary elsewhere. By expanding the second integrand, Eq. (24) leads to

$$J = \int_A \left(\sigma_{ij} \frac{\partial u_i}{\partial x_1} - W\delta_{1j} \right) \frac{\partial q}{\partial x_j} \mathrm{d}A + \int_A \left(\frac{\partial \sigma_{ij}}{\partial x_j} \frac{\partial u_i}{\partial x_1} + \sigma_{ij} \frac{\partial^2 u_i}{\partial x_j \partial x_1} - \sigma_{ij} \frac{\partial \varepsilon_{ij}}{\partial x_1} - \frac{1}{2} \varepsilon_{ij} \frac{\partial D_{ijkl}}{\partial x_1} \varepsilon_{kl} \right) q \, \mathrm{d}A \quad , \tag{25}$$

Using equilibrium ($\partial \sigma_{ij}/\partial x_j = 0$) and strain–displacement ($\varepsilon_{ij} = \partial u_i/\partial x_j$) conditions and noting that $\partial D_{ijkl}/\partial x_1 = 0$ in homogenous orthotropic materials, the second integrand of Eq. (25) vanishes, yielding

$$J = \int_A \left(\sigma_{ij} \frac{\partial u_i}{\partial x_1} - W\delta_{1j} \right) \frac{\partial q}{\partial x_j} \mathrm{d}A \quad , \tag{26}$$

which is the classical domain form of the *J*-integral in homogenous materials.

Consider two independent equilibrium states of the cracked body. Let state 1 correspond to the *actual* state for the given boundary conditions, and let state 2 correspond to an *auxiliary* state, which can be either mode-I or mode-II near tip displacement and stress fields in an orthotropic elastic medium. Superposition of these two states leads to another equilibrium state (state *S*) for which the domain form of the *J*-integral is

$$J^{(S)} = \int_A \left[\left(\sigma_{ij}^{(1)} + \sigma_{ij}^{(2)} \right) \frac{\partial \left(u_i^{(1)} + u_i^{(2)} \right)}{\partial x_1} - W^{(s)} \delta_{1j} \right] \times \frac{\partial q}{\partial x_j} \mathrm{d}A \quad , \tag{27}$$

where superscript i = 1, 2, and *S* indicate fields and quantities associated with state i and

$$W^{(S)} = \frac{1}{2} \left(\sigma_{ij}^{(1)} + \sigma_{ij}^{(2)} \right) \left(\varepsilon_{ij}^{(1)} + \varepsilon_{ij}^{(2)} \right) \quad . \tag{28}$$

By expanding Eqs. (27),

$$J^{(S)} = J^{(1)} + J^{(2)} + M^{(1,2)} \quad , \tag{29}$$

where

$$J^{(1)} = \int_A \left[\sigma_{ij}^{(1)} \frac{\partial u_i^{(1)}}{\partial x_1} - W^{(1)} \delta_{1j} \right] \frac{\partial q}{\partial x_j} \mathrm{d}A \tag{30}$$

and

$$J^{(2)} = \int_A \left[\sigma_{ij}^{(2)} \frac{\partial u_i^{(2)}}{\partial x_1} - W^{(2)} \delta_j \right] \frac{\partial q}{\partial x_j} \mathrm{d}A \tag{31}$$

are the *J*-integrals for states 1 and 2, respectively, and

$$M^{(1,2)} = \int_A \left[\sigma_{ij}^{(1)} \frac{\partial u_i^{(2)}}{\partial x_1} + \sigma_{ij}^{(2)} \frac{\partial u_i^{(1)}}{\partial x_1} - W^{(1,2)} \delta_{1j} \right] \frac{\partial q}{\partial x_j} \mathrm{d}A \tag{32}$$

is an interaction integral. In Eqs. (30–32), $W^{(1)} = \frac{1}{2} \sigma_{ij}^{(1)} \varepsilon_{ij}^{(1)}$, $W^{(2)} = \frac{1}{2} \sigma_{ij}^{(2)} \varepsilon_{ij}^{(2)}$, and $W^{(1,2)} = \frac{1}{2} (\sigma_{ij}^{(1)} \varepsilon_{ij}^{(2)} + \sigma_{ij}^{(2)} \varepsilon_{ij}^{(1)})$ represent various strain energy densities, which satisfy

$$W^{(S)} = W^{(1)} + W^{(2)} + W^{(1,2)} \quad . \tag{33}$$

For linear-elastic homogeneous orthotropic solids under mixed-mode loading conditions, the *J*-integral is also related to the stress intensity factors as

$$J = \alpha_{11} K_I^2 + \alpha_{12} K_I K_{II} + \alpha_{22} K_{II}^2 \quad , \tag{34}$$

where

$$\alpha_{11} = -\frac{a_{22}}{2} \mathrm{Im} \left(\frac{\mu_1 + \mu_2}{\mu_1 \mu_2} \right) \quad , \tag{35}$$

$$\alpha_{22} = \frac{a_{11}}{2} \mathrm{Im} (\mu_1 + \mu_2) \quad , \tag{36}$$

and

$$\alpha_{12} = -\frac{a_{22}}{2} \mathrm{Im} \left(\frac{1}{\mu_1 \mu_2} \right) + \frac{a_{11}}{2} \mathrm{Im} (\mu_1 \mu_2) \quad . \tag{37}$$

Applying Eq. (34) to states 1, 2, and the superimposed state *S* gives

$$J^{(1)} = \alpha_{11} K_I^{(1)^2} + \alpha_{12} K_I^{(1)} K_{II}^{(1)} + \alpha_{22} K_{II}^{(1)^2} \quad , \tag{38}$$

$$J^{(2)} = \alpha_{11} K_I^{(2)^2} + \alpha_{12} K_I^{(2)} K_{II}^{(2)} + \alpha_{22} K_{II}^{(2)^2} \quad , \tag{39}$$

and

$$\begin{aligned} J^{(S)} &= \alpha_{11} \left(K_I^{(1)} + K_I^{(2)} \right)^2 + \alpha_{12} \left(K_I^{(1)} + K_I^{(2)} \right) \left(K_{II}^{(1)} + K_{II}^{(2)} \right) + \alpha_{22} \left(K_{II}^{(1)} + K_{II}^{(2)} \right)^2 \\ &= \alpha_{11} K_I^{(1)^2} + \alpha_{12} K_I^{(1)} K_{II}^{(1)} + \alpha_{22} K_{II}^{(1)^2} + \alpha_{11} K_I^{(2)^2} \\ &\quad + \alpha_{12} K_I^{(2)} K_{II}^{(2)} + \alpha_{22} K_{II}^{(2)^2} + 2\alpha_{11} K_I^{(1)} K_I^{(2)} \\ &\quad + \alpha_{12} \left(K_I^{(1)} K_{II}^{(2)} + K_I^{(2)} K_{II}^{(1)} \right) + 2\alpha_{22} K_{II}^{(1)} K_{II}^{(2)} \\ &= J^{(1)} + J^{(2)} + 2\alpha_{11} K_I^{(1)} K_I^{(2)} \\ &\quad + \alpha_{12} \left(K_I^{(1)} K_{II}^{(2)} + K_I^{(2)} K_{II}^{(1)} \right) + 2\alpha_{22} K_{II}^{(1)} K_{II}^{(2)} \end{aligned} \tag{40}$$

Comparing Eqs. (29) and (40),

$$M^{(1,2)} = 2\alpha_{11} K_I^{(1)} K_I^{(2)} + \alpha_{12} \left(K_I^{(1)} K_{II}^{(2)} + K_I^{(2)} K_{II}^{(1)} \right) + 2\alpha_{22} K_{II}^{(1)} K_{II}^{(2)} \quad . \tag{41}$$

The individual SIFs for the actual state can be obtained by judiciously choosing the auxiliary state (state 2). For example, if state 2 is chosen to be state I, i.e., the mode-I near tip displacement and stress field is chosen as the auxiliary state, then $K_I^{(2)} = 1$ and $K_{II}^{(2)} = 0$. Hence, Eq. (41) reduces to

$$M^{(1,I)} = 2\alpha_{11} K_I^{(1)} + \alpha_{12} K_{II}^{(1)} \quad . \tag{42}$$

Similarly, if state 2 is chosen to be state II, i.e., the mode-II near tip displacement and stress field is chosen as the auxiliary state, then $K_I^{(2)} = 0$ and $K_{II}^{(2)} = 1$. Following similar considerations,

$$M^{(1,II)} = \alpha_{12} K_I^{(1)} + 2\alpha_{22} K_{II}^{(1)} \quad . \tag{43}$$

The interaction integrals $M^{(1,I)}$ and $M^{(1,II)}$ can be evaluated from Eq. 32. Equations (42) and (43) provide a system of linear algebraic equations which can be solved for SIFs,

$K_I^{(1)}$ and $K_{II}^{(1)}$ under various mixed-mode loading conditions.

3.2
Functionally graded materials

For non-homogeneous materials, even though the equilibrium and strain–displacement conditions are satisfied, the material gradient term of the second integrand of Eq. (25) does not vanish. So Eq. (25) leads to a more general integral, henceforth referred to as the $\tilde{J}$-integral [27], which is

$$\tilde{J} = \int_A \left(\sigma_{ij} \frac{\partial u_i}{\partial x_1} - W\delta_{1j} \right) \frac{\partial q}{\partial x_j} \mathrm{d}A - \int_A \frac{1}{2} \varepsilon_{ij} \frac{\partial D_{ijkl}}{\partial x_1} \varepsilon_{kl} q \, \mathrm{d}A \ . \tag{44}$$

By comparing Eq. (44) to the classical J-integral (see Eq. 26), the presence of material non-homogeneity results in the addition of the second domain integral. Although this integral is negligible for a path very close to the crack tip, it must be accounted for with relatively large integral domains, so that the $\tilde{J}$-integral can be accurately calculated. The $\tilde{J}$-integral in Eq. (44) is actually the first component of the $\mathbf{J}^* = \{J_1^*, J_2^*\}^{\mathrm{T}}$ vector integral (i.e., J_1^*) proposed by Eischen [25]. Hence, $\tilde{J}$ also represents the energy release rate of an elastic body.

In order to derive interaction integral for orthotropic FGMs, consider again actual (state 1), auxiliary (state 2), and superimposed (state S) equilibrium states. For the actual state, Eq. (44) can be directly invoked to represent the $\tilde{J}$-integral. However, a more general form, such as Eq. (24), must be used for auxiliary and superimposed states. For example, the $\tilde{J}$-integral for the superimposed state S can be written as

$$\begin{aligned} \tilde{J}^{(S)} &= \int_A \left(\left(\sigma_{ij}^{(1)} + \sigma_{ij}^{(2)} \right) \frac{\partial \left(u_i^{(1)} + u_i^{(2)} \right)}{\partial x_1} - W^{(S)} \delta_{1j} \right) \frac{\partial q}{\partial x_j} \mathrm{d}A \\ &+ \int_A \frac{\partial}{\partial x_j} \left(\left(\sigma_{ij}^{(1)} + \sigma_{ij}^{(2)} \right) \frac{\partial \left(u_i^{(1)} + u_i^{(2)} \right)}{\partial x_1} - W^{(S)} \delta_{1j} \right) q \, \mathrm{d}A \ . \end{aligned} \tag{45}$$

Clearly, the evaluations of $\tilde{J}^{(2)}$ and the resulting interaction integral depend on how the auxiliary field is defined. There are several options in choosing the auxiliary field. Two methods, developed in this study, are described in the following.

3.2.1
Method I – homogeneous auxiliary field

The method I involves selecting the auxiliary stress and displacement fields in an orthotropic elastic medium given by Eqs. (6–8) and Eqs. (15, 16) and calculating the auxiliary strain field from the symmetric gradient of the auxiliary displacement field. In this approach, the auxiliary stress and strain fields are related through a constant constitutive tensor evaluated at the crack tip. Hence, both equilibrium ($\partial \sigma_{ij}^{(2)} / \partial x_j = 0$) and strain–displacement ($\varepsilon_{ij}^{(2)} = \partial u_i^{(2)} / \partial x_j$) conditions are satisfied in the auxiliary state. However, the non-homogeneous constitutive relation of FGM is not strictly satisfied in the auxiliary state, which would introduce gradients of stress fields as extra terms in the interaction integral.

Using Eq. (33) and invoking both equilibrium and strain-displacement conditions, Eq. (45) can be further simplified to

$$\begin{aligned} \tilde{J}^{(S)} = \int_A \Bigg(& \left(\sigma_{ij}^{(1)} + \sigma_{ij}^{(2)} \right) \frac{\partial \left(u_i^{(1)} + u_i^{(2)} \right)}{\partial x_1} \\ & - (W^{(1)} + W^{(2)} + W^{(1,2)}) \delta_{1j} \Bigg) \frac{\partial q}{\partial x_j} \mathrm{d}A \\ & + \int_A \frac{1}{2} \Bigg[-\varepsilon_{ij}^{(1)} \frac{\partial D_{ijkl}}{\partial x_1} \varepsilon_{kl}^{(1)} + \sigma_{ij}^{(1)} \frac{\partial \varepsilon_{ij}^{(2)}}{\partial x_1} - \frac{\partial \sigma_{ij}^{(2)}}{\partial x_1} \varepsilon_{ij}^{(1)} \\ & + \sigma_{ij}^{(2)} \frac{\partial \varepsilon_{ij}^{(1)}}{\partial x_1} - \frac{\partial \sigma_{ij}^{(1)}}{\partial x_1} \varepsilon_{ij}^{(2)} \Bigg] q \, \mathrm{d}A \ . \end{aligned} \tag{46}$$

By expanding Eq. (46),

$$\tilde{J}^{(S)} = \tilde{J}^{(1)} + \tilde{J}^{(2)} + \tilde{M}^{(1,2)} \ , \tag{47}$$

where

$$\tilde{J}^{(1)} = \int_A \left[\sigma_{ij}^{(1)} \frac{\partial u_i^{(1)}}{\partial x_1} - W^{(1)} \delta_{1j} \right] \frac{\partial q}{\partial x_j} \mathrm{d}A - \int_A \frac{1}{2} \varepsilon_{ij}^{(1)} \frac{\partial D_{ijkl}}{\partial x_1} \varepsilon_{kl}^{(1)} q \, \mathrm{d}A \tag{48}$$

$$\tilde{J}^{(2)} = \int_A \left[\sigma_{ij}^{(2)} \frac{\partial u_i^{(2)}}{\partial x_1} - W^{(2)} \delta_{1j} \right] \frac{\partial q}{\partial x_j} \mathrm{d}A \tag{49}$$

are the $\tilde{J}$-integrals for states 1 and 2, respectively, and

$$\begin{aligned} \tilde{M}^{(1,2)} = & \int_A \left[\sigma_{ij}^{(1)} \frac{\partial u_i^{(2)}}{\partial x_1} + \sigma_{ij}^{(2)} \frac{\partial u_i^{(1)}}{\partial x_1} - W^{(1,2)} \delta_{1j} \right] \frac{\partial q}{\partial x_j} \mathrm{d}A \\ & + \int_A \frac{1}{2} \left[\sigma_{ij}^{(1)} \frac{\partial \varepsilon_{ij}^{(2)}}{\partial x_1} - \frac{\partial \sigma_{ij}^{(2)}}{\partial x_1} \varepsilon_{ij}^{(1)} \right. \\ & \left. + \sigma_{ij}^{(2)} \frac{\partial \varepsilon_{ij}^{(1)}}{\partial x_1} - \frac{\partial \sigma_{ij}^{(1)}}{\partial x_1} \varepsilon_{ij}^{(2)} \right] q \, \mathrm{d}A \end{aligned} \tag{50}$$

is the modified interaction integral for non-homogeneous materials.

3.2.2
Method II - non-homogeneous auxiliary field

The method II entails selecting the auxiliary stress and displacement fields in an orthotropic elastic medium given by Eqs. (6–8) and Eqs. (15, 16) and calculating the auxiliary strain field using the same spatially varying constitutive tensor of FGM. In this approach, the auxiliary stress field satisfies equilibrium ($\partial \sigma_{ij}^{(2)} / \partial x_j = 0$); however, the

auxiliary strain field is not compatible with the auxiliary displacement field ($\varepsilon_{ij}^{(2)} \neq \partial u_i^{(2)} \partial x_j$). If the auxiliary fields are not compatible, extra terms that will arise due to lack of compatibility should be taken into account while evaluating the interaction integral, even though they may not be sufficiently singular in the asymptotic limit to contribute to the value of the integral [30]. Hence, this method also introduces additional terms to the resulting interaction integral.

Following similar considerations, but using only equilibrium condition in the auxiliary state, Eq. (45) can also be simplified to

$$\begin{aligned}\tilde{J}^{(S)} = &\int_A \left(\left(\sigma_{ij}^{(1)} + \sigma_{ij}^{(2)}\right) \frac{\partial\left(u_i^{(1)} + u_i^{(2)}\right)}{\partial x_1} \right. \\ &\left. - (W^{(1)} + W^{(2)} + W^{(1,2)})\delta_{1j} \right) \frac{\partial q}{\partial x_j} \mathrm{d}A \\ &+ \int_A \left(\left(\sigma_{ij}^{(1)} + \sigma_{ij}^{(2)}\right) \left(\frac{\partial^2 u_i^{(2)}}{\partial x_j \partial x_1} - \frac{\partial \varepsilon_{ij}^{(2)}}{\partial x_1} \right) \right. \\ &\left. - \frac{1}{2}\left(\varepsilon_{ij}^{(1)} + \varepsilon_{ij}^{(2)}\right) \frac{\partial D_{ijkl}}{\partial x_1} \left(\varepsilon_{kl}^{(1)} + \varepsilon_{kl}^{(2)}\right) \right) q dA \end{aligned} \tag{51}$$

Comparing Eqs. (47) and (51),

$$\begin{aligned}\tilde{J}^{(1)} = &\int_A \left[\sigma_{ij}^{(1)} \frac{\partial u_i^{(1)}}{\partial x_1} - W^{(1)}\delta_{1j} \right] \frac{\partial q}{\partial x_j} \mathrm{d}A \\ &- \int_A \frac{1}{2} \varepsilon_{ij}^{(1)} \frac{\partial D_{ijkl}}{\partial x_1} \varepsilon_{kl}^{(1)} q \, \mathrm{d}A \end{aligned} \tag{52}$$

$$\begin{aligned}\tilde{J}^{(2)} = &\int_A \left[\sigma_{ij}^{(2)} \frac{\partial u_i^{(2)}}{\partial x_1} - W^{(2)}\delta_{1j} \right] \frac{\partial q}{\partial x_j} \mathrm{d}A \\ &+ \int_A \left[\sigma_{ij}^{(2)} \frac{\partial^2 u_i^{(2)}}{\partial x_j \partial x_1} - \frac{1}{2} \varepsilon_{ij}^{(2)} \frac{\partial D_{ijkl}}{\partial x_1} \varepsilon_{kl}^{(2)} \right] q \, \mathrm{d}A \end{aligned} \tag{53}$$

are the $\tilde{J}$-integrals for states 1 and 2, respectively, and

$$\begin{aligned}\tilde{M}^{(1,2)} = &\int_A \left[\sigma_{ij}^{(1)} \frac{\partial u_i^{(2)}}{\partial x_1} + \sigma_{ij}^{(2)} \frac{\partial u_i^{(1)}}{\partial x_1} - W^{(1,2)}\delta_{1j} \right] \frac{\partial q}{\partial x_j} \mathrm{d}A \\ &+ \int_A \left[\sigma_{ij}^{(1)} \left(\frac{\partial^2 u_i^{(2)}}{\partial x_j \partial x_1} - \frac{\partial \varepsilon_{ij}^{(2)}}{\partial x_1} \right) - \varepsilon_{ij}^{(1)} \frac{\partial D_{ijkl}}{\partial x_1} \varepsilon_{kl}^{(2)} \right] q dA \end{aligned} \tag{54}$$

is another modified interaction integral for non-homogeneous materials. Note that, to evaluate the second integrand of Eq. 54 needs only higher order derivatives of the auxiliary fields, which can be easily obtained from Eqs. (6–20). However to evaluate the second integrand of Eq. (50) needs higher order derivatives of the actual displacement fields also, which requires higher-order elements in FEM and also more computational effort.

Note, for homogeneous materials, $\partial D_{ijkl}/\partial x_1 = 0$, $\varepsilon_{ij}^{(2)} = \partial u_i^{(2)}/\partial x_j$, $\sigma_{ij}^{(1)} \partial \varepsilon_{ij}^{(2)}/\partial x_1 = \partial \sigma_{ij}^{(2)}/\partial x_1 \varepsilon_{ij}^{(1)}$ and $\sigma_{ij}^{(2)} \partial \varepsilon_{ij}^{(1)}/\partial x_1 = \partial \sigma_{ij}^{(1)}/\partial x_1 \varepsilon_{ij}^{(2)}$, regardless of how the auxiliary field is defined. As a result, the $\tilde{J}^{(1)}, \tilde{J}^{(2)}$, and $\tilde{M}^{(1,2)}$ integrals in methods I and II degenerate to their corresponding homogeneous solutions, as expected.

3.2.3 Stress-intensity factors

For linear-elastic solids, the $\tilde{J}-$integral also represents the energy release rate and, hence,

$$\tilde{J} = \alpha_{11,\mathrm{tip}} K_I^2 + \alpha_{12,\mathrm{tip}} K_I K_{II} + \alpha_{22,\mathrm{tip}} K_{II}^2 \ , \tag{55}$$

where $\alpha_{11,\mathrm{tip}}$, $\alpha_{12,\mathrm{tip}}$, and $\alpha_{22,\mathrm{tip}}$ are evaluated at the crack tip. Regardless of how the auxiliary fields are defined, Eq. (55) applied to states 1, 2, and S yields

$$\tilde{J}^{(1)} = \alpha_{11,\mathrm{tip}} K_I^{(1)^2} + \alpha_{12,\mathrm{tip}} K_I^{(1)} K_{II}^{(1)} + \alpha_{22,\mathrm{tip}} K_{II}^{(1)^2} \ , \tag{56}$$

$$\tilde{J}^{(2)} = \alpha_{11,\mathrm{tip}} K_I^{(2)^2} + \alpha_{12,\mathrm{tip}} K_I^{(2)} K_{II}^{(2)} + \alpha_{22,\mathrm{tip}} K_{II}^{(2)^2} \ , \tag{57}$$

and

$$\begin{aligned}\tilde{J}^{(S)} &= \alpha_{11,\mathrm{tip}} \left(K_I^{(1)} + K_I^{(2)}\right)^2 + \alpha_{12,\mathrm{tip}} \left(K_I^{(1)} + K_I^{(2)}\right) \\ &\quad \times \left(K_{II}^{(1)} + K_{II}^{(2)}\right) + \alpha_{22,\mathrm{tip}} \left(K_{II}^{(1)} + K_{II}^{(2)}\right)^2 \\ &= \alpha_{11,\mathrm{tip}} K_I^{(1)^2} + \alpha_{12,\mathrm{tip}} K_I^{(1)} K_{II}^{(1)} + \alpha_{22,\mathrm{tip}} K_{II}^{(1)^2} \\ &\quad + \alpha_{11,\mathrm{tip}} K_I^{(2)^2} + \alpha_{12,\mathrm{tip}} K_I^{(2)} K_{II}^{(2)} + \alpha_{22,\mathrm{tip}} K_{II}^{(2)^2} \\ &\quad + 2\alpha_{11,\mathrm{tip}} K_I^{(1)} K_I^{(2)} + \alpha_{12,\mathrm{tip}} \left(K_I^{(1)} K_{II}^{(2)} + K_I^{(2)} K_{II}^{(1)}\right) \\ &\quad + 2\alpha_{22,\mathrm{tip}} K_{II}^{(1)} K_{II}^{(2)} \\ &= J^{(1)} + J^{(2)} + 2\alpha_{11,\mathrm{tip}} K_I^{(1)} K_I^{(2)} + \alpha_{12,\mathrm{tip}} \\ &\quad \times \left(K_I^{(1)} K_{II}^{(2)} + K_I^{(2)} K_{II}^{(1)}\right) + 2\alpha_{22,\mathrm{tip}} K_{II}^{(1)} K_{II}^{(2)} \ . \end{aligned} \tag{58}$$

Comparing Eqs. (47) and (58),

$$\begin{aligned}\tilde{M}^{(1,2)} = &2\alpha_{11,\mathrm{tip}} K_I^{(1)} K_I^{(2)} + \alpha_{12,\mathrm{tip}} \left(K_I^{(1)} K_{II}^{(2)} + K_I^{(2)} K_{II}^{(1)}\right) \\ &+ 2\alpha_{22,\mathrm{tip}} K_{II}^{(1)} K_{II}^{(2)} \ . \end{aligned} \tag{59}$$

Following a similar procedure and judiciously choosing the intensity of the auxiliary state as described earlier, the SIFs for non-homogenous materials can also be derived as

$$\tilde{M}^{(1,I)} = 2\alpha_{11,\mathrm{tip}} K_I^{(1)} + \alpha_{12,\mathrm{tip}} K_{II}^{(1)} \ , \tag{60}$$

and

$$\tilde{M}^{(1,II)} = \alpha_{12,\mathrm{tip}} K_I^{(1)} + 2\alpha_{22,\mathrm{tip}} K_{II}^{(1)} \ , \tag{61}$$

where $\tilde{M}^{(1,I)}$ and $\tilde{M}^{(1,II)}$ are two modified interaction integrals for modes I and II, respectively. The interaction integrals $\tilde{M}^{(1,I)}$ and $\tilde{M}^{(1,II)}$ can be evaluated using either Eq. (50) or Eq. (54) depending on the auxiliary field. Equations (60) and (61) provide a system of linear algebraic equations which can be solved for SIFs $K_I^{(1)}$ and $K_{II}^{(1)}$ under various mixed-mode loading conditions. Both methods

developed in this study were used in performing numerical calculations, to be presented in a forthcoming section.

Note, Eqs. (60) and (61) are the result of a simple generalization of the interaction integral method for calculating fracture parameters in linear-elastic non-homogenous materials. When both the elastic modulus and the Poisson's ratio have no spatial variation, $\tilde{M}^{(1,2)} = M^{(1,2)}$. Consequently, Eqs. (60) and (61) degenerate into Eqs. (42) and (43), as expected.

4
Numerical examples

The newly modified interaction integrals (methods I and II) developed in this study were applied to evaluate the SIFs of cracks in othrotropic FGMs. Both single- (mode I) and mixed-mode (modes I and II) conditions were considered and three examples are presented here. The proposed two interaction integrals (methods I and II) are fairly domain independent, however in all the examples a domain ($2b_1 \times 2b_2$), with size $2b_1 = 2b_2 =$ crack length $2a$ surrounding each crack tip is chosen for evaluating the integrals. The results obtained in the current study were compared with the semi-analytical solutions by Ozturk and Erdogan [35, 36]. For the sake of comparison the independent engineering constants, $E_{11}, E_{22}, G_{12}, \nu_{12},$ and ν_{21} are replaced by a stiffness parameter E, a stiffness ratio δ^4, an average Poisson's ratio ν , and a shear parameter κ [35, 36], which are defined as

$$E = \sqrt{E_{11}E_{22}}, \quad \delta^4 = \frac{E_{11}}{E_{22}} = \frac{\nu_{12}}{\nu_{21}}, \qquad \nu = \sqrt{\nu_{12}\nu_{21}}, \quad \kappa = \frac{E}{2G_{12}} - \nu \ , \tag{62}$$

for plane stress, and

$$E = \sqrt{\frac{E_{11}E_{22}}{(1-\nu_{13}\nu_{31})(1-\nu_{23}\nu_{32})}}, \quad \delta^4 = \frac{E_{11}}{E_{22}}\frac{(1-\nu_{23}\nu_{32})}{(1-\nu_{13}\nu_{31})}, \qquad \nu = \sqrt{\frac{(\nu_{12}+\nu_{13}\nu_{32})(\nu_{21}+\nu_{23}\nu_{31})}{(1-\nu_{13}\nu_{31})(1-\nu_{23}\nu_{32})}}, \quad \kappa = \frac{E}{2G_{12}} - \nu \tag{63}$$

for plane strain.

4.1
Example 1: plate with an interior crack parallel to material gradation under mode-I

Consider an orthotropic square plate of dimensions $2L = 2W = 20$ units ($L/W = 1$) with a central crack of length $2a = 2.0$ units, subjected to crack-face pressure loading, as shown in Fig. 2a. A plane stress condition was assumed. The crack is parallel to the material gradation and the following material property data were employed for FEM analysis: $E_{11}(x_1) = E_{11}^0 e^{\beta x_1}$, $E_{22}(x_1) = E_{22}^0 e^{\beta x_1}$, $G_{12}(x_1) = G_{12}^0 e^{\beta x_1}$, where the average modulus of elasticity $E(x_1) = E^0 e^{\beta a(x_1/a)}$, with $E^0 = \sqrt{E_{11}^0 E_{22}^0}$. The non-homogeneity parameter βa is varied from 0.0 to 1.0. Two different values of the shear parameter $\kappa = -0.25$ and 5.0 were employed. The stiffness ratio $\delta^4 = 0.25$ and the average Poisson's ratio $\nu = 0.3$ were used in the FEM analysis.

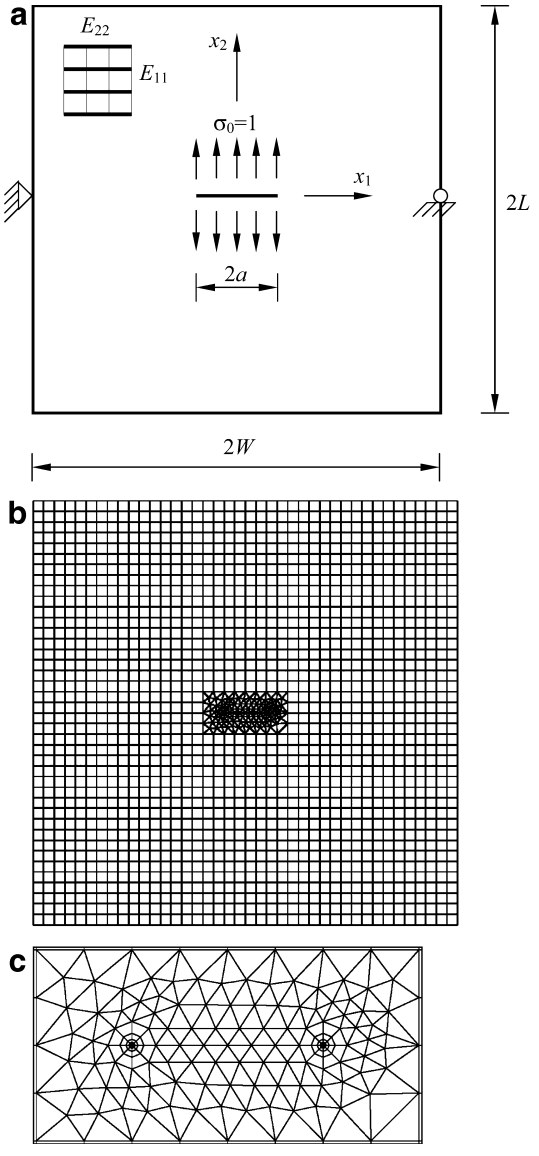

Fig. 2. Plate with an interior crack parallel to material gradation under mode-I: **a** geometry and loads; **b** FEM discretization (5756 nodes, 1696 8-noded quadrilateral elements, 214 6-noded triangular elements, and 16 focused quarter-point 6-noded triangular elements); and **c** enlarged view of discretization around the crack tips

The applied load corresponds to σ_{22} $(-1 \le x_1 \le 1, \pm 0) = \pm\sigma_0 = \pm 1.0$ along top and bottom crack faces. The displacement boundary condition is prescribed such that $u_1 = u_2 = 0$ for the node in the middle of the left edge, and $u_2 = 0$ for the node in the middle of the right edge. The FEM discretization involves 5756 nodes, 1696 8-noded quadrilateral elements, 214 6-noded triangular elements, and 8 focused quarter-point 6-noded triangular elements in the vicinity of each crack tip, as shown in Fig. 2b. Figure 2c depicts the enlarged view of discretization around the crack tips. A 2×2 Gaussian integration was employed.

Ozturk and Erdogan [35] investigated an infinite plate with the same configuration. Obviously, a FEM model cannot represent the infinite domains addressed in the analysis of Ozturk and Erdogan [35], but as long as the

Table 1. Normalized stress intensity factors for an orthotropic plate under uniform crack face pressure loading ($\kappa = -0.25$)

βa	Proposed method-I $\left[\tilde{M}^{(1,2)}\right]$		Proposed method-II $\left[\tilde{M}^{(1,2)}\right]$		Ozturk and Erdogan [35]	
	$\frac{K_I(a)}{\sigma_0\sqrt{\pi a}}$	$\frac{K_I(-a)}{\sigma_0\sqrt{\pi a}}$	$\frac{K_I(a)}{\sigma_0\sqrt{\pi a}}$	$\frac{K_I(-a)}{\sigma_0\sqrt{\pi a}}$	$\frac{K_I(a)}{\sigma_0\sqrt{\pi a}}$	$\frac{K_I(-a)}{\sigma_0\sqrt{\pi a}}$
0.0	1.0003	1.0003	1.0009	1.0008	1.0	1.0
0.01	1.0013	0.9997	1.0016	1.0005	1.0025	0.9975
0.1	1.0176	0.9689	1.0354	0.9844	1.0246	0.9747
0.25	1.0587	0.9335	1.0770	0.9497	1.0604	0.9364
0.50	1.1099	0.8699	1.1297	0.8823	1.1177	0.8740
0.75	1.1709	0.8099	1.1695	0.8169	1.1720	0.8154
1.00	1.2287	0.7703	1.2137	0.7621	1.2235	0.7616
1.50	1.2999	0.6698	1.3065	0.6722	1.3184	0.6701
2.00	1.3899	0.5909	1.3908	0.6016	1.4043	0.5979

ratios a/W and a/L are kept relatively small (e.g, $a/W = a/L \leq 1/10$), the approximation is acceptable. Tables 1 and 2 provide a comparison between predicted normalized stress intensity factors $K_I(a)\sigma_0\sqrt{\pi a}$ and $K_I(-a)/\sigma_0\sqrt{\pi a}$ at both crack tips for several values of non-homogeneous parameter βa, obtained by proposed interaction integral methods I and II, and those of Ozturk and Erdogan [35] for shear parameters $\kappa = -0.25$ and 5.0, respectively. The numerical results from proposed methods I and II shows that effect of κ on normalized stress intensity factors is less significant than that of βa. Also the stress intensity factor on the stiffer side of the medium is always greater than that on the less stiff side. The agreement between the present results of proposed methods and Ozturk and Erdogan's [35] analytical solution is excellent, regardless of methods I and II.

Table 2. Normalized stress intensity factors for an orthotropic plate under uniform crack face pressure loading ($\kappa = 5.0$)

βa	Proposed method-I $\left[\tilde{M}^{(1,2)}\right]$		Proposed method-II $\left[\tilde{M}^{(1,2)}\right]$		Ozturk and Erdogan [35]	
	$\frac{K_I(a)}{\sigma_0\sqrt{\pi a}}$	$\frac{K_I(-a)}{\sigma_0\sqrt{\pi a}}$	$\frac{K_I(a)}{\sigma_0\sqrt{\pi a}}$	$\frac{K_I(-a)}{\sigma_0\sqrt{\pi a}}$	$\frac{K_I(a)}{\sigma_0\sqrt{\pi a}}$	$\frac{K_I(-a)}{\sigma_0\sqrt{\pi a}}$
0.0	0.9967	0.9967	1.0005	1.0005	1.0	1.0
0.01	1.0014	1.0002	1.0052	1.0049	1.0025	0.9975
0.1	1.0199	0.9833	1.0247	0.9867	1.0231	0.9733
0.25	1.0499	0.9289	1.0587	0.9289	1.0531	0.9306
0.50	1.0961	0.8543	1.0887	0.8602	1.0946	0.8594
0.75	1.1203	0.7878	1.1301	0.8069	1.1281	0.7932
1.00	1.1499	0.7298	1.1603	0.7363	1.1556	0.7339
1.50	1.2007	0.6295	1.2015	0.6401	1.1979	0.6367
2.00	1.2305	0.5586	1.2307	0.5598	1.2290	0.5636

4.2
Example 2: plate with an interior crack perpendicular to material gradation (mixed mode)

Consider an orthotropic square plate of dimensions $2L = 2W = 20$ units ($L/W = 1$) with a central crack of length $2a = 2.0$ units, as shown in Fig. 3. Except for material properties and loading conditions, all other conditions including FEM discretization were same as in Example 1. However, the crack is perpendicular to the material gradation. In Example 2, both crack-face pressure loading and crack-face shear loading were considered separately. The following material property data were employed for FEM analysis: $E_{11}(x_2) = E_{11}^0 e^{\beta x_2}$, $E_{22}(x_2) = E_{22}^0 e^{\beta x_2}$, $G_{12}(x_2) = G_{12}^0 e^{\beta x_2}$, where the average modulus of elasticity $E(x_2) = E^0 e^{\beta a(x_2/a)}$, with $E^0 = \sqrt{E_{11}^0 E_{22}^0}$. The non-homogeneity parameter βa is varied from 0.0 to 2.0. Two different values of the shear parameter $\kappa = 0.5$ and 5.0 and two different stiffness ratio $\delta^4 = 0.25$, and 10 were employed in the FEM analysis. Three different values of the average Poisson's ratio $\nu = 0.15, 0.30,$ and 0.45 were used in the computations.

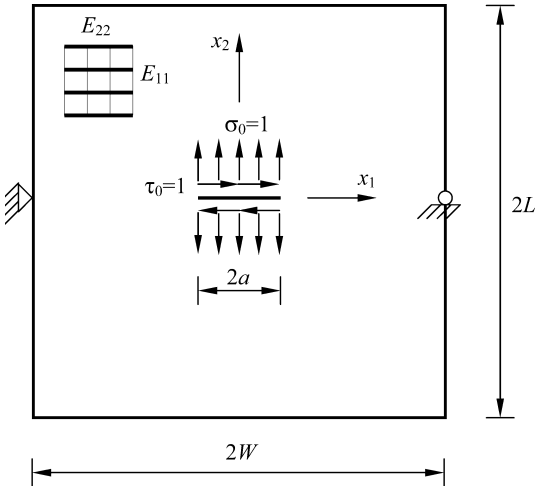

Fig. 3. Plate with an interior crack perpendicular to material gradation: geometry and loads

For crack-face pressure loading the applied load corresponds to $\sigma_{22}(-1 \leq x_1 \leq 1, \pm 0) = \pm\sigma_0 = \pm 1.0$ and for crack-face shear loading the applied load corresponds to $\sigma_{12}(-1 \leq x_1 \leq 1, \pm 0) = \pm\tau_0 = \pm 1.0$ along top and bottom crack faces. A 2×2 Gaussian integration was adopted.

The effect of the non-homogeneity parameter βa and effect of the average Poisson's ratio ν on the normalized stress intensity factors for both crack-face pressure loading and crack-face shear loading were studied. The present results obtained by proposed interaction integral methods I and II are compared with those reported by Ozturk and Erdogan [36], who investigated an infinite plate with the same configuration. Tables 3 and 4 provide a comparison between predicted normalized stress intensity factors under uniform crack-face pressure loading and uniform crack-face shear loading, respectively, obtained by proposed interaction integral methods I and II, and those

Table 3. The effect of the non-homogeneity parameter on the normalized stress intensity factors for an orthotropic plate under uniform crack face pressure loading ($\delta^4 = 0.25$, ν=0.3, $\kappa = 0.5$)

βa	Proposed method-I $\left[\tilde{M}^{(1,2)}\right]$		Proposed method-II $\left[\tilde{M}^{(1,2)}\right]$		Ozturk and Erdogan [36]	
	$\frac{K_I(a)}{\sigma_0\sqrt{\pi a}}$	$\frac{K_{II}(a)}{\sigma_0\sqrt{\pi a}}$	$\frac{K_I(a)}{\sigma_0\sqrt{\pi a}}$	$\frac{K_{II}(a)}{\sigma_0\sqrt{\pi a}}$	$\frac{K_I(a)}{\sigma_0\sqrt{\pi a}}$	$\frac{K_{II}(a)}{\sigma_0\sqrt{\pi a}}$
0.0	1.0067	0.0	1.0059	0.0	1.0	0.0
0.1	1.0206	0.0248	1.0193	0.0246	1.0115	0.0250
0.25	1.0502	0.0599	1.0513	0.0609	1.0489	0.0627
0.50	1.1373	0.1303	1.1355	1.1299	1.1351	0.1263
1.00	1.3398	0.2497	1.3406	0.2501	1.3494	0.2587
2.00	1.8623	0.5493	1.8598	0.5564	1.8580	0.5529

Table 4. The effect of the non-homogeneity parameter on the normalized stress intensity factors for an orthotropic plate under uniform crack face shear loading ($\delta^4 = 0.25$, ν=0.3, $\kappa = 0.5$)

βa	Proposed method-I $\left[\tilde{M}^{(1,2)}\right]$		Proposed method-II $\left[\tilde{M}^{(1,2)}\right]$		Ozturk and Erdogan [36]	
	$\frac{K_I(a)}{\tau_0\sqrt{\pi a}}$	$\frac{K_{II}(a)}{\tau_0\sqrt{\pi a}}$	$\frac{K_I(a)}{\tau_0\sqrt{\pi a}}$	$\frac{K_{II}(a)}{\tau_0\sqrt{\pi a}}$	$\frac{K_I(a)}{\tau_0\sqrt{\pi a}}$	$\frac{K_{II}(a)}{\tau_0\sqrt{\pi a}}$
0.0	0.0	0.9998	0.0	1.0007	0.0	1.0
0.1	−0.0487	1.0005	−0.0496	0.9999	−0.0494	0.9989
0.25	−0.1156	0.9971	−0.1167	0.9973	−0.1191	0.9968
0.50	−0.2196	0.9964	−0.2203	0.9969	−0.2217	0.9965
1.00	−0.3874	0.9999	−0.3799	1.0006	−0.3862	1.0071
2.00	−0.5698	1.0399	−0.5708	1.0453	−0.5725	1.0499

of Ozturk and Erdogan [36] for various values of non-homogeneity parameter βa, and $\delta^4 = 0.25$; $\nu = 0.3$; and $\kappa = 0.5$. Tables 5 and 6 provide a comparison between predicted normalized stress intensity factors under uniform crack face pressure loading for $\delta^4 = 0.25$, and $\delta^4 = 10$ respectively, obtained by proposed interaction integral methods I and II, and those of Ozturk and Erdogan [36] for $\nu = 0.15, 0.3$, and 0.45 and $\beta a = 0.5$, and 1.0. Tables 7 and 8 provide a similar comparison for an orthotropic plate under uniform crack face shear loading. The agreement between the results of the proposed methods and Ozturk and Erdogan's [36] analytical solution is excellent, irrespective of methods I and II.

4.3 Example 3: slanted crack in a plate under mixed-mode

Consider a centrally located, inclined crack of length $2a = 2\sqrt{2}$ units in a finite two-dimensional orthotropic rectangular plate of size $2L = 40$ units and $2W = 20$ units, as shown in Fig. 4a. A plane stress condition was assumed. This example is investigated with material variation following exponential functions and the following material property data were used for FEM analysis: $E_{11}(x_1) = E^0_{11}e^{\alpha x_1}$, $E_{22}(x_1) = E^0_{22}e^{\beta x_1}$, $G_{12}(x_1) = G^0_{12}e^{\gamma x_1}$, $E^0_{11} = 3.5 \times 10^6$, $E^0_{22} = 12 \times 10^6$, $G^0_{12} = 3 \times 10^6$, $\nu_{12} = 0.204$, and $E_{11}/E_{22} = \nu_{12}/\nu_{21}$. The following two cases were examined: (1) an orthotropic FGM with proportional material variation $(\alpha, \beta, \gamma) = (0.2, 0.2, 0.2)$, and (2) an orthotropic FGM with non-proportional material variation $(\alpha, \beta, \gamma) = (0.5, 0.4, 0.3)$.

The applied load corresponds to σ_{22} $(-10 \le x_1 \le 10, \pm 20) = \pm\sigma^\infty = \pm 1.0$ along top and bottom edges. The displacement boundary condition is prescribed such that $u_1 = u_2 = 0$ for the node in the middle of the left edge, and $u_2 = 0$ for the node in the middle of the right edge. The FEM discretization involves 3606 Nodes, 898 8-noded quadrilateral elements, 354 6-noded triangular elements, and 8 focused quarter-point 6-noded triangular elements in the vicinity of each crack tip, as shown in Fig. 4b. Figure 4c depicts the enlarged view of discretization around the crack tips.

Table 9 provides a comparison between predicted SIFs $K_I^+(a)$, $K_{II}^+(a)$, $K_I^-(a)$, and $K_{II}^-(a)$ at both crack tips, obtained by proposed interaction integral methods I and II, and existing results obtained by Kim and Paulino from the literature [37]. A good agreement is obtained between the results of the proposed methods and Kim and Paulino's [37] numerical results by using the MCC and DCT.

Table 5. The effect of the Poisson's ratio on the normalized stress intensity factors for an orthotropic plate under uniform crack face pressure loading ($\kappa = 5.0$)

βa	$\delta^4 = 0.25$	Proposed method-I $\left[\tilde{M}^{(1,2)}\right]$			Proposed method-II $\left[\tilde{M}^{(1,2)}\right]$			Ozturk and Erdogan [36]		
	ν	0.15	0.30	0.45	0.15	0.30	0.45	0.15	0.30	0.45
0.5	$K_I(a)/\sigma_0\sqrt{\pi a}$	1.2531	1.2578	1.2599	1.2528	1.2583	1.2608	1.2516	1.2596	1.2674
	$K_{II}(a)/\sigma_0\sqrt{\pi a}$	0.1217	0.1219	0.1219	0.1267	0.1270	0.1271	0.1259	0.1259	0.1259
1.0	$K_I(a)/\sigma_0\sqrt{\pi a}$	1.5603	1.5729	1.5845	1.5599	1.5748	1.5836	1.5589	1.5739	1.5884
	$K_{II}(a)/\sigma_0\sqrt{\pi a}$	0.2600	0.2599	0.2516	0.2583	0.2581	0.2499	0.2555	0.2557	0.2558

Table 6. The effect of the Poisson's ratio on the normalized stress intensity factors for an orthotropic plate under uniform crack face pressure loading ($\kappa = 5.0$)

βa	$\delta^4 = 10$	Proposed method-I $\left[\tilde{M}^{(1,2)}\right]$			Proposed method-II $\left[\tilde{M}^{(1,2)}\right]$			Ozturk and Erdogan [36]		
	ν	0.15	0.30	0.45	0.15	0.30	0.45	0.15	0.30	0.45
0.5	$K_I(a)/\sigma_0\sqrt{\pi a}$	1.0699	1.0720	1.0799	1.0710	1.0716	1.0810	1.0748	1.0776	1.0804
	$K_{II}(a)/\sigma_0\sqrt{\pi a}$	0.1239	0.1252	0.1259	0.1227	0.1248	0.1256	0.1252	0.1252	0.1251
1.0	$K_I(a)/\sigma_0\sqrt{\pi a}$	1.1889	1.1955	1.2009	1.1897	1.1993	1.2056	1.1892	1.1955	1.2017
	$K_{II}(a)/\sigma_0\sqrt{\pi a}$	0.2499	0.2503	0.2536	0.2538	0.2543	0.2537	0.2511	0.2512	0.2512

Table 7. The effect of the Poisson's ratio on the normalized stress intensity factors for an orthotropic plate under uniform crack face shear loading ($\kappa = 5.0$)

βa	$\delta^4 = 0.25$	Proposed method-I $\left[\tilde{M}^{(1,2)}\right]$			Proposed method-II $\left[\tilde{M}^{(1,2)}\right]$			Ozturk and Erdogan [36]		
	v	0.15	0.30	0.45	0.15	0.30	0.45	0.15	0.30	0.45
0.5	$K_I(a)/\tau_0\sqrt{\pi a}$	−0.1926	−0.1909	−0.1900	−0.1956	−0.1945	−0.1923	−0.1980	−0.1971	−0.1963
	$K_{II}(a)/\tau_0\sqrt{\pi a}$	0.9899	0.9907	0.9960	0.9888	0.9999	0.9919	0.9898	0.9915	0.9931
1.0	$K_I(a)/\tau_0\sqrt{\pi a}$	−0.3199	−0.3099	−0.3067	−0.3199	−0.3056	−0.3048	−0.3203	−0.3186	−0.3169
	$K_{II}(a)/\tau_0\sqrt{\pi a}$	0.9899	0.9901	0.9968	0.9901	0.9953	0.9968	0.9888	0.9921	0.9953

Table 8. The effect of the Poisson's ratio on the normalized stress intensity factors for an orthotropic plate under uniform crack face shear loading ($\kappa = 5.0$)

βa	$\delta^4 = 10$	Proposed method-I $\left[\tilde{M}^{(1,2)}\right]$			Proposed method-II $\left[\tilde{M}^{(1,2)}\right]$			Ozturk and Erdogan [36]		
	v	0.15	0.30	0.45	0.15	0.30	0.45	0.15	0.30	0.45
0.5	$K_I(a)/\tau_0\sqrt{\pi a}$	−0.0359	−0.0379	−0.0380	−0.0360	−0.0383	−0.0383	−0.0366	−0.0365	−0.0365
	$K_{II}(a)/\tau_0\sqrt{\pi a}$	0.9909	0.9911	0.9925	0.9911	0.9917	0.9977	0.9956	0.9961	0.9965
1.0	$K_I(a)/\tau_0\sqrt{\pi a}$	−0.0659	−0.0649	−0.0627	−0.0655	−0.0648	−0.0631	−0.0660	−0.0657	−0.0654
	$K_{II}(a)/\tau_0\sqrt{\pi a}$	0.9899	0.9905	0.9917	0.9898	0.9913	0.9949	0.9913	0.9925	0.9938

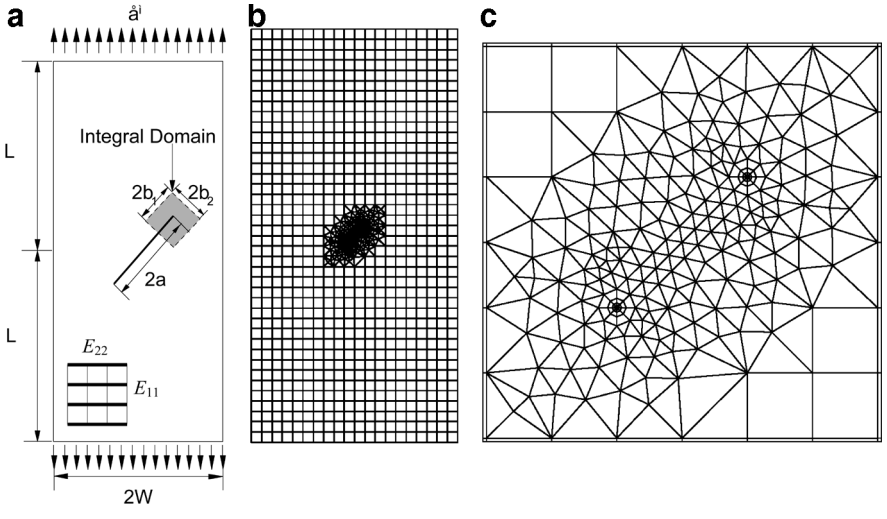

Fig. 4. Slanted crack in a plate under mixed-mode: **a** geometry and loads; **b** FEM discretization (3606 Nodes, 898 8-noded quadrilateral elements, 354 6-noded triangular elements, and 16 focused quarter-point 6-noded triangular elements); and **c** enlarged view of discretization around the crack tips

Table 9. Mixed-mode stress-intensity factor in an orthotropic functionally graded plate with a slant crack

Material	Method	$K_I^+(a)$	$K_{II}^+(a)$	$K_I^-(a)$	$K_{II}^-(a)$
FGM (proportional) $(\alpha, \beta, \gamma) = (0.2, 0.2, 0.2)$	Kim and Paulino (MCC) [37]	1.762	1.439	1.403	1.288
	Kim and Paulino (DCT) [37]	1.769	1.419	1.419	1.284
	Proposed Method-I $\left[\tilde{M}^{(1,2)}\right]$	1.728	1.429	1.411	1.299
	Proposed Method-II $\left[\tilde{M}^{(1,2)}\right]$	1.725	1.432	1.409	1.300
FGM (non-proportional) $(\alpha, \beta, \gamma) = (0.5, 0.4, 0.3)$	Kim and Paulino (MCC) [37]	2.384	1.581	1.437	1.225
	Kim and Paulino (DCT) [37]	2.387	1.553	1.456	1.229
	Proposed Method-I $\left[\tilde{M}^{(1,2)}\right]$	2.393	1.603	1.399	1.217
	Proposed Method-II $\left[\tilde{M}^{(1,2)}\right]$	2.399	1.611	1.407	1.204

5 Summary and conclusions

Two new interaction integrals have been developed for calculating stress-intensity factors for a stationary crack in two-dimensional orthotropic functionally graded materials of arbitrary geometry. The method involves finite element discretization, where the material properties are smooth functions of spatial co-ordinates and two newly developed interaction integrals for mixed-mode fracture analysis. The proposed interaction integral can also be implemented in conjunction with other numerical methods, such as meshless method, boundary element method, and other.

Three numerical examples, including both mode-I and mixed-mode problems, are presented to evaluate the accuracy of fracture parameters calculated by the proposed interaction integrals. Comparisons have been made between the stress-intensity factors predicted by the proposed interaction integrals and available reference solutions in the literature, generated either analytically or numerically using various other fracture integrals or analyses. An excellent agreement is obtained between the results of proposed interaction integrals and the previously obtained solutions.

References

1. **Suresh S, Mortensen A** (1998) Fundamentals of functionally graded materials. IOM Communications Ltd., London
2. **Hirano T, Teraki J, Yamada T** (1990) On the design of functionally gradient materials. In: Yamanouochi M, Koizumi M, Hirai T, Shiota I (eds), Proceedings of the First International Symposium on Functionally Gradient Materials, Sendai, Japan, pp. 5–10
3. **Igari T, Notomi A, Tsunoda H, Hida K, Kotoh T, Kunishima S** (1990) Material properties of functionally gradient material for fast breeder reactor. In: Yamanouochi M, Koizumi M, Hirai T, Shiota I (eds), Proceedings of the First International Symposium on Functionally Gradient Materials, Sendai, Japan, pp. 209–214
4. **Tani J, Liu GR** (1993) Surface waves in functionally gradient piezoelectric plates. JSME Int. J. Series A (Mechanics and Material Engineering), 36(2): 152–155
5. **Osaka T, Matsubara H, Homma T, Mitamura S, Noda K** (1990) Microstructural study of electroless-plated CoNiReP/NiMoP double-layered media for perpendicular magnetic recording. Japanese J. Appl. Phys. 29(10): 1939–1943
6. **Watanabe Y, Nakamura Y, Fukui Y, Nakanishi K** (1993) A magnetic-functionally graded material manufactured with deformation-induced martensitic transformation. J. Mater. Sci. Lett. 12(5): 326–328
7. **Koike Y** (1992) Graded-index and single mode polymer optical fibers, In: Chiang LY, Garito AG, Sandman DJ (eds), Electrical, Optical, and Magnetic Properties of Organic Solid State Materials, Materials Research Proceedings, Pittsburgh, PA, MRS, Vol. 247, p. 817
8. **Desplat JL** (1996) Recent developments on oxygenated thermionic energy converter-overview. Proceedings of the Fourth International Symposium on Functionally Graded Materials, Tsukuba City, Japan
9. **Oonishi H, Noda T, Ito S, Kohda A, Yamamoto H, Tsuji E** (1994) Effect of hydroxyapatite coating on bone growth into porous titanium alloy implants under loaded conditions. J. Appl. Biomater. 5(1): 23–27
10. **Getto H, Ishihara S** (1996) Development of the fire retardant door with functionally gradient wood. Proceedings of the Fourth International Symposium on Functionally Graded Materials, Tsukuba City, Japan
11. **Erdogan F** (1995) Fracture mechanics of functionally graded materials. Comput. Eng. 5(7): 753–770
12. **Gibson RE** (1967) Some results concerning displacements and stresses in a nonhomogeneous elastic half space. Geotechnique 17: 58–67
13. **Delale F, Erdogan F** (1983) The crack problem for a nonhomogeneous plane. J. Appl. Mech. 50: 609–614
14. **Erdogan F, Wu BH** (1993) Analysis of FGM specimens for fracture toughness testing. Proceedings of the Second International Symposium on Functionally Graded Materials, Ceramic Transactions, Westerville, Ohio, The American Ceramic Society, 34: 39–46
15. **Marur PR, Tippur HV** (2000) Numerical analysis of crack tip fields in functionally graded materials with a crack normal to the elastic gradient. Int. J. Solids Struct. 37: 5353–5370
16. **Noda N, Jin ZH** (1993) Thermal stress intensity factors for a crack in a strip of a functionally graded materials. Int. J. Solids Struct. 30: 1039–1056
17. **Jin ZH, Noda N** (1993) An internal crack parallel to the boundary of a nonhomogeneous half plane under thermal loading. Int. J. Eng. Sci. 31: 793–806
18. **Erdogan F, Wu BH** (1996) Crack problems in FGM layers under thermal stresses. J. Ther. Stresses 19: 237–265
19. **Jin ZH, Batra RC** (1996) Stress intensity relaxation at the tip of an edge crack in a functionally graded material subjected to a thermal shock. J. Ther. Stresses 19: 317–339
20. **Wang BL, Han JC, Du SY** (2000) Crack problems for functionally graded materials under transient thermal loading. J. Ther. Stresses 23(2): 143–168
21. **Jin ZH, Paulino GH** (2001) Transient thermal stress analysis of an edge crack in a functionally graded material. Int. J. Fract. 107(1): 73–98
22. **Wang BL, Noda N** (2001) Thermal induced fracture of a smart functionally graded composite structure. Theor. Appl. Fract. Mech. 35(2): 93–109
23. **Anlas G, Santare MH, Lambros J** (2000) Numerical calculation of stress intensity factors in functionally graded materials. Int. J. Fract. 104: 131–143
24. **Chen J, Wu L, Du S** (2000) Element free galerkin methods for fracture of functionally graded materials. Key Eng. Mater. 183–187: 487–492
25. **Eischen JW** (1987) Fracture of nonhomogeneous materials. Int. J. Fract. 34: 3–22
26. **Kim JH, Paulino GH** (2002) Finite element evaluation of mixed mode stress intensity factors in functionally graded materials. Int. J. Numer. Meth. Eng. 53(8): 1903–1935
27. **Gu P, Dao M, Asaro RJ** (1999) A simplified method for calculating the crack tip field of functionally graded materials using the domain integral. J. Appl. Mech. 66: 101–108
28. **Bao G, Wang L** (1995) Multiple cracking in functionally graded ceramic/metal coatings. Int. J. Solids Struct. 32(19): 2853–2871
29. **Bao G, Cai H** (1997) Delamination cracking in functionally graded coating/metal substrate systems. Acta Mechanica 45(3): 1055–1066
30. **Rao BN, Rahman S** (2003) Meshfree analysis of cracks in isotropic functionally graded materials. Eng. Fract. Mech. 70: 1–27
31. **Dolbow JE, Gosz M** (2002) On the computation of mixed-mode stress intensity factors in functionally graded materials. Int. J. Solids Struct. 39(9): 2557–2574
32. **Sampath S, Herman H, Shimoda N, Saito T** (1995) Thermal spray processing of FGMs. M.R.S. Bulletin 20(1): 27–31
33. **Kaysser WA, Ilschner B** (1995) FGM research activities in Europe. M.R.S. Bulletin 20(1): 22–26
34. **Gu P, Asaro RJ** (1997) Cracks in functionally graded materials. Int. J. Solids Struct. 34: 1–17
35. **Oztuk M, Erdogan F** (1997) Mode I crack problem in an inhomogeneous orthotropic medium. Int. J. Eng. Sci. 35(9): 869–883
36. **Oztuk M, Erdogan F** (1999) The mixed mode crack problem in an inhomogeneous orthotropic medium. Int. J. Fract. 98: 243–261
37. **Kim JH, Paulino GH** (2002) Mixed-mode fracture of orthotropic functionally graded materials using finite elements and the modified crack closure method. Eng. Fract. Mech. 69: 1557–1586
38. **Lekhnitskii SG, Tsai SW, Cheron T** (1986) Anisotropic Plates. Gorden and Breach Science Publishers, New York

39. **Shih GC, Paris PC, Irwin GR** (1965) On cracks in rectilinearly anisotropic bodies. Int. J. Fract. 1: 189–203
40. **Yau JF, Wang SS, Corten HT** (1980) A mixed-mode crack analysis of isotropic solids using conservation laws of elasticity. J. Appl. Mech. 47: 335–341
41. **Wang SS, Yau JF, Corten HT** (1980) A mixed-mode crack analysis of rectilinear anisotropic solids using conservation laws of elasticity. Int. J. Fract. 16(3): 247–259
42. **Rice JR** (1968) A path independent integral and the approximate analysis of strain concentration by notches and cracks. J. Appl. Mech. 35: 379–386
43. **Moran B, Shih F** (1987) Crack tip and associated domain integrals from momentum and energy balance. Eng. Fract. Mech. 27: 615–642